ACES Asian Chemical Editorial Society

DOI: 10.1002/asia.201900301

CHEMISTRY AN ASIAN JOURNAL Full Paper

SPECIAL ISSUE

Rolled-Up Monolayer Graphene Tubular Micromotors: Enhanced Performance and Antibacterial Property

Biran Zhang,[a] Gaoshan Huang,[a] Lu Wang,[a] Tianbo Wang,[b] Lu Liu,[c, d] Zengfeng Di,[b] Xuanyong Liu,[c] and Yongfeng Mei*[a]

Abstract: The motion of catalytic tubular micromotors are driven by the oxygen bubbles generated from chemical reaction and is influenced by the resistance from the liquid environment. Herein, we fabricated a rolled-up graphene tubular micromotor, in which the graphene layer was adopted as the outmost surface. Due to the hydrophobic property of the graphene layer, the fabricated micromotor performed a motion pattern that could escape from the attraction from the bubbles. In addition, *Escherichia coli* and *Staphylococcus* culture experiments proved that the graphene outer surface displays antibacterial property. Considering the bubble-avoiding and antibacterial properties, the rolled-up graphene tubular micromotor holds great potential for various applications such as in vivo drug delivery and biosensors.

Introduction

Artificial self-propelled machines at the micro/nanoscale with various structures, for example, bi-metal rods,[1] Janus particles,[2] tubes,[3] and helixes,[4] have drawn much attention over the past decade. Among those different structures, micro/nanotubes are studied for their asymmetric inner and outer surfaces.[5] In 2009, we brought up the concept of catalytic tubular microrockets fabricated by rolled-up nanotechnology, which set up the foundation of catalytic tubular micromachines.[3a] Oxygen bubbles produced by H_2O_2 catalytical decomposition on the inner surface with catalytic property, such as for example, Pt, Ag, and catalase, eject from one end of the tubular structure, and propel the tubular micromotor to move forward. Micromotor with this driving fashion was soon developed to be a promising candidate in multiple applications, such as cargo delivery and releasing,[6] environmental remediation,[7] bio-sensing,[8] etc. In most applications, the ability of avoiding the interference from surrounding environment like bubbles is required.[9] Especially, the micromotor attached to the large bubble will be hard to escape from the surface tension of the bubble. In most cases, surfactants are added in the H_2O_2 solution to decrease the surface tension of the inner wall and to increase the bubble propulsion frequency of micromotors. The correspondingly decreased size of oxygen bubbles leads to reduced influence from bubbles as obstacles.[6a,10] However, surfactants can only decrease the size but not the amount of the bubbles, and micromotors are still hindered by the small bubbles in surrounding environment. In addition, ultrasonication was also used to removing oxygen bubbles generated from the catalytic reaction. Nevertheless, the fast elimination of oxygen bubbles propelled led to decreased micromotors' speed.[11]

Graphene is a promising two dimensional material with outstanding electronic and optical properties.[12] Numerous studies on applications of graphene in flexible electronic devices,[13] molecule detecting,[14] and energy storage[15] have been published. Previous studies have combined graphene-based materials and tubular micromotors to take advantage of the excellent properties of graphene and its derivations and explored new applications for micromotors. In general, two approaches are engaged for the fabrication of tubular micromotors, i,e., rolled-up nanotechnology and template-assisted fabrication, and the rolled-up nanotechnology has the advantage of producing tubular structures with various materials and their combinations.[5] Graphene-related micromotors were previously fabricated via both approaches.[16] For instance, Y. P. Zhao et al.[16a] reported a graphene oxide (GO)/Ti/Pt tubular micromotor fabricated by rolled-up nanotechnology, where sonica-

[a] B. R. Zhang, G. S. Huang, L. Wang, Y. F. Mei
Department of Materials Science
State Key Laboratory of ASIC and Systems
Fudan University
Shanghai 200433 (China)
E-mail: yfm@fudan.edu.cn

[b] T. B. Wang, Prof. Z. F. Di
State Key Laboratory of Functional Materials for Informatics
Shanghai Institute of Microsystem and Technology
Chinese Academy of Sciences
Shanghai 200050 (China)

[c] L. Liu, X. Y. Liu
State Key Laboratory of High Performance Ceramics and Superfine Microstructure
Shanghai Institute of Ceramics
Chinese Academy of Sciences
Shanghai 200050 (China)

[d] L. Liu
State Key Laboratory of Resource Chemistry of Ministry of Education
Shanghai Key Laboratory of the Rare Earth Functional Materials
Shanghai Municipal Education Committee Key Laboratory of Molecular Imaging Probes and Sensors
Shanghai Normal University
Shanghai 200234 (China)

Supporting information and the ORCID identification number(s) for the author(s) of this article can be found under: https://doi.org/10.1002/asia.201900301.

This manuscript is part of a special issue on Smart Chemistry, Smart Motors. Click here to see the Table of Contents of the special issue.

tion was used to break the weak bond between the substrate and the GO nanosheet. On the other hand, J. Wang's group introduced a template-assisted electrodeposited graphene/Pt micromotor.[16c] GO was electrochemically reduced when it was electrodeposited on the inner surface of a porous polycarbonate membrane. In addition, other carbon materials (like C_{60} fullerene, carbon nanotube, graphene, and carbon black) may also be incorporated into the tubular micromotors by template-assisted electrodeposition.[17] It is worth noting that studies in the past have theoretically and experimentally proven that graphene is hydrophobic.[18] Here we take advantage of the hydrophobicity of monolayer graphene and use it as the outmost layer of tubular micromotor. This structure can be conveniently achieved by the rolled-up nanotechnology. The outer surface of the micromotor has less interaction with the hydrophilic groups on the outer surface of the obstacle. In this work, we noticed that the rolled-up graphene micromotor could move through a string of bubbles and bypass a large bubble with the size comparable to that of the micromotor. The speed of graphene micromotor experienced a temporary decrease, but recovered rapidly as soon as it departed from the bubbles.

In addition, among various promising applications of micromotors, in vivo application is one of the most remarkable ones because this can relived people from agony of surgeries and some side effects of drugs.[19] However, micromotors as a foreign substance entering the human body may bring infectious agents like bacteria. In this case, micromotors with antibacterial property would much improve the situation. Researchers have reported the antibacterial property of graphene and graphene derivatives.[20] The antibacterial property of graphene based materials is considered as a result of (1) oxidative stress that can interfere with the metabolism of bacteria associated with reactive oxygen species or charge transfer generated by graphene; (2) physical harm to bacteria cell membranes by the sharp edges of graphene nanoflakes that lead to the leakage of intracellular substances; and (3) graphene as a flexible thin film wrapping and trapping bacteria cell membrane.[20a,d,21] In order to verify the antibacterial property of our graphene tubular micromotors, we cultured the micromotors with *Escherichia coli* (*E. coli*) and *Staphylococcus* (*S. aureus*) on Ge substrate. By analyzing the surviving situation of bacteria on graphene covered surface and area without graphene, we proved that the outer surface of tubular micromotors could prevent bacteria multiply. With hydrophobic and antibacterial surface, this rolled-up monolayer graphene tubular micromotor could have great potentials for in vivo applications as man-made micro/nanomachines.

Results and Discussion

The catalytic tubular graphene micromotor was fabricated by rolled-up technology,[22] as illustrated in Figure 1 a. The monolayer graphene was first grown on Ge substrate by chemical vapor deposition (CVD) with H_2 and CH_4.[23] Then, Ti and Cr layers were deposited on graphene sequentially by e-beam evaporation with differed deposition rates and thicknesses, which introduced internal strain into the multilayer nanomembrane system.[22a] The e-beam evaporation was also used to deposit a thin Pt layer for about 2 nm to be the inner catalytic layer of the tubular micromotor. Thus, graphene/Ti/Cr/Pt four-layered nanomembrane was fabricated. Later on, a standard photolithography procedure followed by ion beam etching (IBE) was applied to create patterns on graphene/Ti/Cr/Pt nanomembrane. Afterwards, the remained photoresist was removed by acetone and Ge substrate was partially etched by H_2O_2 solution so the graphene/Ti/Cr/Pt nanomembrane was released and rolled up under the control of the built-in strain. At last, critical point drying was engaged in order to prevent structure collapse caused by the surface tension of liquid. For comparison, micromotor without graphene decoration was also prepared. In such case, the outer surface of the micromotor is Ti.

The obtained rolled-up tubular micromotors were characterized by scanning electron microscopy (SEM) and the results are shown in Figure 1 b. The two pits under the rolled-up micro-

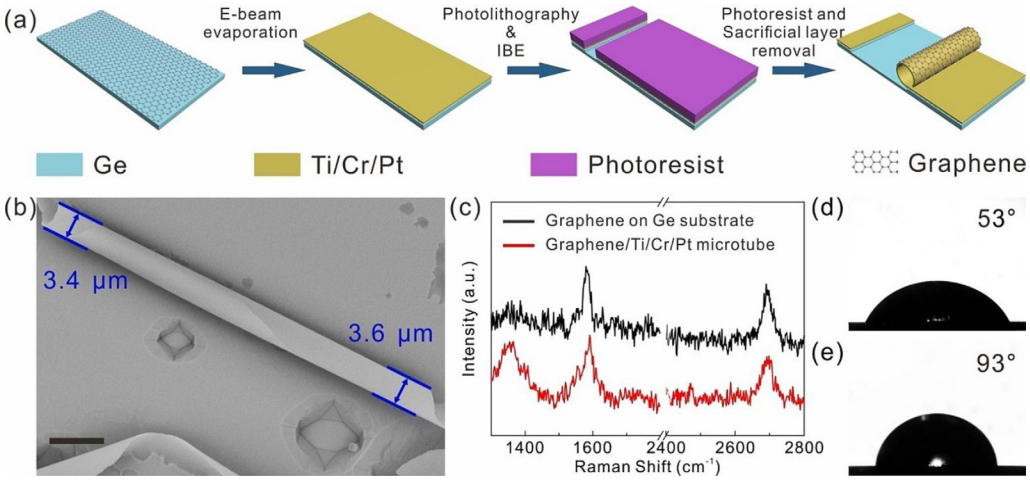

Figure 1. (a) Schematic of fabrication process of the rolled-up graphene/Ti/Cr/Pt tubular micromotor. (b) SEM image of a rolled-up tubular micromotor. The diameters of both ends of the tubular micromotor are marked. Scale bar: 10 μm (c) Raman spectra of graphene on Ge substrate (black) and the rolled-up graphene/Ti/Cr/Pt microtube (red). The contact angle of (d) 20 nm Ti nanomembrane and (e) single layer graphene.

tube was generated from the anisotropic corrosion on the single crystal Ge substrate by H_2O_2 solution.[24] The fabricated micromotor has a fine and straight tubular structure with the diameters of 3.4 and 3.6 μm for left and right ends (Figure 1b), respectively. Here, due to the imperfection of the rolling process, the diameter of the right end is slightly larger than the diameter of the left end. This asymmetry is actually important for micromotor application, since the generated oxygen on the inner surface of the micromotor would gather to form bubbles and migrate to the lager end under the influence of capillary force.[25] In addition, energy-dispersive X-ray spectroscopy (EDX) mappings of the samples were carried out to check the elemental distribution, and typical results are presented in Figure S1. One can see that Ti and Cr distribute evenly on the tube wall. While the Ge signal is slightly weakened on the position of the tubular micromotor, for that the micromotor shields part of the Ge signal. However, the monolayer graphene and Pt layer (≈2 nm) are too thin for EDX signal collection. In order to prove the existence of graphene layer, Raman spectroscopy was adopted. Figure 1c demonstrates the Raman spectra of bare graphene on Ge substrate (black line) and the rolled-up graphene/Ti/Cr/Pt microtube (red line), which indicates the existence of graphene on the outer surface of the rolled-up tubular micromotors. In addition, it could be noticed in Figure 1c that the characteristic peaks of graphene microtube has a slight blue shift compared to those of planar graphene. This phenomenon indicates that the graphene layer is in compression due to the rolling process, which leads to blue shift of Raman characteristic peaks.[26] In addition, the wettabilities of the outer surfaces of micromotors were studied by means of contact angle (CA) measurement. As shown in Figure 1d and e, the CAs of flat monolayer graphene and Ti nanomembrane are 53° and 93°, respectively, proving that the Ti surface is hydrophilic and monolayer graphene surface is hydrophobic.

When H_2O_2 solution as the fuel was filled in the microtube and catalytically decomposed on inner Pt surface, the generated O_2 bubbles thrusted out from larger end of the tubular structure and propelled the tubular micromotor to move forward. In present work, the motion behavior of the fabricated graphene micromotor in H_2O_2 solution was characterized in detail by optical microscopy, as shown in Figure 2a and b. The optical images in Figure 2a show the circular motion of a tubular graphene micromotor with a speed of ≈612 μm s^{-1} in

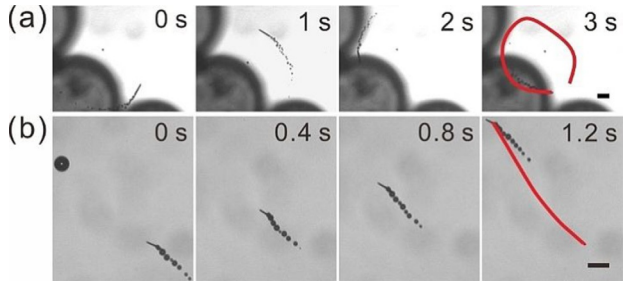

Figure 2. Circular motion (a) and linear motion (b) of graphene micromotors in solution of 15% H_2O_2 and 0.01 wt.% SDBS. Scale bar: 100 μm.

15% H_2O_2 and 0.01 wt.% surfactant (Sodium dodecylbenzenesulfonate, SDBS) solution. The red line denotes the motion trajectory in 3 s. Linear motion of a graphene micromotor was also observed in Figure 2b, with a speed of ≈602 μm s^{-1} in the solution of the same composition. Time lapse images of a fast motion of a graphene micromotor at a speed of ≈1667 μm s^{-1} in solution with higher H_2O_2 concentration are also presented in Figure S2. Theoretically, tubular micromotors would have linear motions by the driving force generated from the ejection of bubbles, whose direction is along the central axis of the tubular structure. However, the rolled-up procedure is not always ideally controlled, which leads to imperfection of the tubular structure. The flaws of the structure of micromotors such as the opening not being perfectly circle would much influence the motion trajectory, resulting in the circular motion.[16a,27] In addition, physical changes of the liquid environment such as the excitation of eddy flow will also lead to the motion trajectory change of micromotors.[28]

Figure 3a and b show the motion behaviors of micromotors with and without graphene at the outer surfaces. In Figure 3a, the micromotor without graphene modified surface moving with bubbles attach to its surface. In Figure 3a, one can see

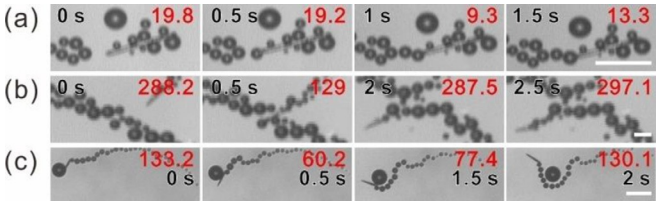

Figure 3. (a) Time lapse images of micromotor without graphene covered moving with bubbles attached. (b) Time lapse images of graphene micromotor moving through a string of bubbles without bubbles attached to its surface. (c) Time lapse images of graphene micromotor encountered a large bubble and bypassed it. Scale bar: 100 μm. The red numbers denote the instantaneous speed of the micromotors.

that the motion speed of the micromotor without graphene decoration reduces from 19.2 to 13.3 μm s^{-1} in 1.5 s, demonstrating a speed loss of more than 30% after the attachment of the bubble. The influence of the bubble as obstacle is remarkable. On the other hand, it could be noticed that for the micromotor with graphene decoration, no bubble is attached to the surface of the micromotor when it moves through a string of bubbles (Figure 3b). The images in Figure 3b show that when the graphene micromotor encountered the bubbles, the motion speed rapidly decrease to less than half of the original speed. After ≈2 s, the micromotor passes through the string of the bubbles, and the motion speed quickly recovers to the original value. Figure 3c denotes a graphene micromotor bypassing a large bubble in its motion trajectory. When the graphene micromotor meets the bubble, the motion is hampered and speed decreased to less than 50%. Propelled by the ejection of oxygen bubbles, the graphene micromotor moves around the large bubble for more than a semi-circumference, then escapes from the micromotor-bubble interaction. The quick speed recovery after detachment can also be observed

in this case. It should be pointed out that high concentration of H_2O_2 was used in current experiments for better demonstrating the interaction between the hydrophobic surface of graphene micromotor and bubbles. However, for potential biomedical applications, rolled-up tubular micromotors have the ability of moving in H_2O_2 with low concentration.[6a, 29]

Another advantage of graphene that has caught great attention is its antibacterial property. Experiments were carried out to characterize the antibacterial property of graphene/Ti/Cr/Pt tubular micromotors. Here, *E. coli* and *S. aureus* culture solution was dropped on the micromotors. After 24 h of culture, the sample was lyophilized to avoid deformation of micromotors and bacteria. Then SEM images were taken to characterize bacteria surviving situation. In Figure 4a-i, the bacteria in red circle have blurred edges and abnormal round shapes, compared with healthy rod-shape *E. coli* on the substrate, indicating that the bacteria are dead. Figure 4a-ii shows that bacteria can survive on the inner surface of the four-layered graphene/Ti/Cr/Pt nanomembrane, which is Pt and is not covered by graphene, and no *E. coli* can be observed on the outer graphene surface. This strongly proves the antibacterial property of graphene micromotor. Figure 4a-iii shows a micromotor with *S. aureus* growing on the inner surface (see red circle) but the graphene covered outer surface is smooth without bacteria. More experimental results demonstrating that bacteria can attach on the inner surfaces of graphene micromotors but not on the outer surfaces are presented in Figure S3. All these experimental results indicate that bacteria can hardly stick on the outer surface of graphene micromotors and multiply. In order to further prove the antibacterial property of the graphene micromotors, we applied fluorescent staining experiments on graphene micromotors, micromotors without graphene, and Si wafer,[30] and the results are shown in Figure 4b. In Figure 4b-i, an obvious blank area with tubular shape corresponding to graphene micromotor can be distinguished, and only a few bacteria can attach on the surface of the graphene micromotor. However, in Figure 4b-ii, considerably more bacteria attach on the surface of the micromotor without graphene, indicating that graphene has the ability of prohibiting *E. coli* from attaching on its surface. While in Figure 4b-iii, the bright stains indicating that the bacteria can attach and multiply on Si wafer. Here, for the mechanism of antibacterial behavior, we believe that neither sharp edge incising mechanism nor wrapping and trapping mechanism is suitable for graphene outer surface, and the death of bacteria co-cultured with graphene micromotors were caused mainly by oxidative stress generated by graphene.[18a,d, 19] The antibacterial property of graphene micromotors demonstrates great potential for in vivo applications.

Conclusions

In conclusion, we rolled up monolayer graphene with a metallic nanomembrane by strain engineering to fabricate a tubular micromotor with enhanced performance and antibacterial property. The hydrophobicity of graphene relieved the motion of the micromotor from being interfered by the bubbles in its trajectory, and a quick speed recovery was observed. Furthermore, the antibacterial property of the graphene micromotor was verified and culture experiments demonstrated that the bacteria were either killed by graphene or could not attach to the graphene surface. This kind of tubular catalytic micromotors is expected to be of importance for in vivo applications, such as drug delivery and minimally invasive surgery.

Experimental Section

Synthesis of monolayer graphene

Ge wafers (175 μm, ATX) were used as the substrates to carry out graphene synthesis in an ambient pressure CVD system. Firstly the Ge substrates were surrounded by the atmosphere of Ar and H_2 with flow rate ratio of 700:70 sccm to wait for the furnace heated to 916 °C. Then CH_4 was filled in to start graphene growth with flow rate of 2.2 sccm at 916 °C for 240 min, while H_2 and Ar were kept the same flow rate. At last, furnace was turned off and cooled to room temperature as CH_4 flow was cut to 0 sccm and H_2 and Ar were remain unchanged.

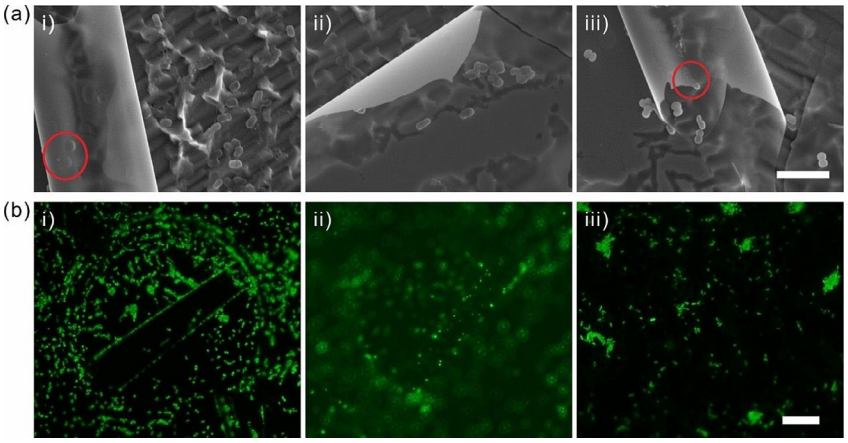

Figure 4. (a) SEM images of graphene micromotors on Ge substrate co-culture with (i) and (ii) *E. coli* and (iii) *S. aureus*. (i) Dead *E. coli* on the outer surface of the micromotor. (ii) A rolled four-layered graphene/Ti/Cr/Pt nanomembrane with *E. coli* on the inner surface. (iii) *S. aureus* on the inner surface of the micromotor and un-rolled nanomembrane on the substrate. Scale bar: 5 μm. (b) Fluorescent images of bacteria on i) graphene micromotor, ii) micromotor without graphene, and iii) Si wafer. Scale bar: 25 μm.

Fabrication of rolled-up graphene micromotors

After monolayer graphene was grown on Ge substrate, Ti/Cr/Pt nanomembrane was deposited sequentially by e-beam evaporation with thicknesses of 10/10/2 nm and deposition rate of 2.0/1.0/0.1 Å s^{-1}. This procedure was carried out on electron beam evaporator (Tenstar TSV700, China). The change in deposition rates endowed the metal nanomembrane with built-in strain. Next, photoresist layer with patterns that had specific size and shape was obtained on the upmost Ti layer by conventional photolithography. Then, Ti, Cr, Pt, graphene, and part of the Ge substrate that were not covered by photoresist was removed by Ar ion beam etching (AdvancedMEMS IBE, China). To release the four-layered nanomembrane from the substrate, 30% H_2O_2 purchased from Sinopharm Chemical Reagen Co., Ltd was used to etch the Ge substrate at 90 °C. After Ge substrate was partially etched, tubular structure of the nanomembrane was formed. The whole sample with substrate was then transferred into pure ethanol and then drying was performed in a critical point dryer (CPD030, Leica, Germany).

Morphology and optical characterizations of rolled-up tubular micromotors

The morphologies of the fabricated tubular micromotors was characterized by scanning electron microscope (Thermo Fisher Scientific Phenom proX desktop SEM, USA). Raman spectra of the synthesized monolayer graphene and the fabricated tubular micromotors were obtained on a Horiba Jobin Yvon HR-Evolution 2 model to confirm the existence of graphene on micromotors. The distribution of elements on the sample was observed by EDX spectroscopy (IXRF-550i, IXRF systems, USA).

Characterizations of the motion of micromotors

The micromotors were transferred to H_2O_2 solution by scratching the substrate using a tapped microcapillary. The motions of the micromotors were observed and recorded by an optical microscope (Olympus BX51TRF, Japan).

Antibacterial property characterization

E. coli (ATCC25922) and *S. aureus* (ATCC25923) were used in the experiments. A few drops of bacterial suspension (10^{-7} cfu mL^{-1}) was dropped on the Ge substrate with rolled-up tubular graphene micromotors and incubated for 24 h at 37 °C. SEM images of the samples after culture experiment were taken on a scanning electron microscopy (HITACHI S3400, Japan). For fluorescent experiment, the bacteria were stain by the LIVE/DEAD BacLight Kit (L13152). The samples were rinsed twice by normal saline after being cultured for 24 h at 37 °C. Then the dye was dropped on each sample and stained for 15 min. At last, the samples were observed by a fluorescence microscope (GX71, Olympus, Japan).

Acknowledgements

This work is supported by the Natural Science Foundation of China (Nos. 51475093, 61628401, and U1632115), Science and Technology Commission of Shanghai Municipality (No. 17JC1401700), and the Changjiang Young Scholars Program of China. Part of the experimental work has been carried out in the Fudan Nanofabrication Laboratory.

Conflict of interest

The authors declare no conflict of interest.

Keywords: antibacterial property · catalytic motion · graphene · hydrophobic effect · micromotors

[1] a) G. A. Ozin, I. Manners, S. Fournier-Bidoz, A. Arsenault, *Adv. Mater.* **2005**, *17*, 3011 – 3018; b) D. Kagan, P. Calvo-Marzal, S. Balasubramanian, S. Sattayasamitsathit, K. M. Manesh, G.-U. Flechsig, J. Wang, *J. Am. Chem. Soc.* **2009**, *131*, 12082 – 12083.
[2] a) M. N. Popescu, S. Dietrich, M. Tasinkevych, J. Ralston, *Eur. Phys. J. E* **2010**, *31*, 351 – 367; b) X. Ma, K. Hahn, S. Sanchez, *J. Am. Chem. Soc.* **2015**, *137*, 4976 – 4979; c) N. Guarrotxena, O. García, I. Quijada-Garrido, *Sci. Rep.* **2018**, *8*, 5721.
[3] a) A. A. Solovev, Y. F. Mei, E. B. Ureña, G. S. Huang, O. G. Schmidt, *Small* **2009**, *5*, 1688 – 1692; b) W. Gao, S. Sattayasamitsathit, J. Orozco, J. Wang, *J. Am. Chem. Soc.* **2011**, *133*, 11862 – 11864.
[4] a) A. Ghosh, P. Fischer, *Nano Lett.* **2009**, *9*, 2243 – 2245; b) W. Gao, X. M. Feng, A. Pei, C. R. Kane, R. Tam, C. Henness, J. Wang, *Nano Lett.* **2014**, *14*, 305 – 310.
[5] B. R. Xu, B. R. Zhang, L. Wang, G. S. Huang, Y. F. Mei, *Adv. Funct. Mater.* **2018**, *28*, 1705872.
[6] a) A. A. Solovev, S. Sanchez, M. Pumera, Y. F. Mei, O. G. Schmidt, *Adv. Funct. Mater.* **2010**, *20*, 2430 – 2435; b) M. Medina-Sánchez, L. Schwarz, A. K. Meyer, F. Hebenstreit, O. G. Schmidt, *Nano Lett.* **2016**, *16*, 555 – 561; c) S. Sattayasamitsathit, H. H. Kou, W. Gao, W. Thavarajah, K. Kaufmann, L. F. Zhang, J. Wang, *Small* **2014**, *10*, 2830 – 2833.
[7] a) W. Gao, X. M. Feng, A. Pei, Y. E. Gu, J. X. Li, J. Wang, *Nanoscale* **2013**, *5*, 1325 – 1331; b) L. Soler, V. Magdanz, V. M. Fomin, S. Sanchez, O. G. Schmidt, *ACS Nano* **2013**, *7*, 9611 – 9620; c) B. Jurado-Sánchez, J. Wang, *Environ. Sci.: Nano* **2018**, *5*, 1530 – 1544.
[8] a) M. García, J. Orozco, M. Guix, W. Gao, S. Sattayasamitsathit, A. Escarpa, A. Merkoçi, J. Wang, *Nanoscale* **2013**, *5*, 1325 – 1331; b) B. Jurado-Sánchez, *Biosensors* **2018**, *8*, 59; c) Q. Yang, J. H. Li, X. Y. Wang, H. L. Peng, H. Xiong, L. X. Chen, *Biosens. Bioelectron.* **2018**, *112*, 54 – 71.
[9] G. S. Huang, J. Y. Wang, Z. Q. Liu, D. K. Zhou, Z. A. Tian, B. R. Xu, L. Q. Li, Y. F. Mei, *Nanoscale* **2017**, *9*, 18590 – 18596.
[10] a) K. M. Manesh, M. Cardona, R. Yuan, M. Clark, D. Kagan, S. Balasubramanian, J. Wang, *ACS Nano* **2010**, *4*, 1799 – 1804; b) R. Mohammadi, J. Wassink, A. Amirfazli, *Langmuir* **2004**, *20*, 9657 – 9662.
[11] T. L. Xu, F. Soto, W. Gao, V. Garcia-Gradilla, J. X. Li, X. J. Zhang, J. Wang, *J. Am. Chem. Soc.* **2014**, *136*, 8552 – 8555.
[12] a) K. S. Novoselov, A. K. Geim, S. V. Morozov, D. Jiang, Y. Zhang, S. V. Dubonos, I. V. Grigorieva, A. A. Firsov, *Science* **2004**, *306*, 666 – 669; b) A. C. Ferrari, J. C. Meyer, V. Scardaci, C. Casiraghi, M. Lazzeri, F. Mauri, S. Piscanec, D. Jiang, K. S. Novoselov, S. Roth, A. K. Geim, *Phys. Rev. Lett.* **2006**, *97*, 187401; c) Y. W. Zhu, S. Murali, W. W. Cai, X. S. Li, J. W. Suk, J. R. Potts, R. S. Ruoff, *Adv. Mater.* **2010**, *22*, 3906 – 3924.
[13] a) H. Gwon, H.-S. Kim, K. U. Lee, D.-H. Seo, Y. C. Park, Y.-S. Lee, B. T. Ahn, K. Kang, *Energy Environ. Sci.* **2011**, *4*, 1277 – 1283; b) K. S. Kim, Y. Zhao, H. Jang, S. Y. Lee, J. M. Kim, K. S. Kim, J.-H. Ahn, P. Kim, J.-Y. Choi, B. H. Hong, *Nature* **2009**, *457*, 706 – 710.
[14] a) F. Schedin, A. K. Geim, S. V. Morozov, E. W. Hill, P. Blake, M. I. Katsnelson, K. S. Novoselov, *Nat. Mater.* **2007**, *6*, 652 – 655; b) S. Kumar, W. Ahlawat, R. Kumar, N. Dilbaghi, *Biosens. Bioelectron.* **2015**, *70*, 498 – 503; c) S. M. Feng, M. C. dos Santos, B. R. Carvalho, R. T. Lv, Q. Li, K. Fujisawa, A. L. Elías, Y. Lei, N. Perea-López, M. Endo, M. H. Pan, M. A. Pimenta, M. Terrones, *Sci. Adv.* **2016**, *2*, e1600322.
[15] a) Z. Zhang, L.-L. Kong, S. Liu, G.-R. Li, X.-P. Gao, *Adv. Energy Mater.* **2017**, *7*, 1602543; b) M. D. Stoller, S. Park, Y. W. Zhu, J. An, R. S. Ruoff, *Nano Lett.* **2008**, *8*, 3498 – 3502.
[16] a) K. Yao, M. Manjare, C. A. Barrett, B. Yang, T. T. Salguero, Y. P. Zhao, *J. Phys. Chem. Lett.* **2012**, *3*, 2204 – 2208; b) L. Baptista-Pires, J. Orozco, P. Guardia, A. Merkoçi, *Small* **2018**, *14*, 1702746; c) A. Martín, B. Jurado-Sánchez, A. Escarpa, J. Wang, *Small* **2015**, *11*, 3568 – 3574; d) D. Vilela, J. Parmar, Y. F. Zeng, Y. L. Zhao, S. Sánchez, *Nano Lett.* **2016**, *16*, 2860 –

2866; e) H. Ye, J. Kang, G. F. Ma, H. Q. Sun, S. B. Wang, *J. Colloid Interface Sci.* **2018**, *528*, 271 – 280.
[17] R. Maria-Hormigos, B. Jurado-Sanchez, L. Vazquez, A. Escarpa, *Chem. Mater.* **2016**, *28*, 8962 – 8970.
[18] a) O. Leenaerts, B. Partoens, F. M. Peeters, *Phys. Rev. B* **2009**, *79*, 235440; b) S. R. Wang, Y. Zhang, N. Abidi, L. Cabrales, *Langmuir* **2009**, *25*, 11078 – 11081.
[19] a) W. Gao, R. F. Dong, S. Thamphiwatana, J. X. Li, W. W. Gao, L. F. Zhang, J. Wang, *ACS Nano* **2015**, *9*, 117 – 123; b) B. Esteban-Fernández de Ávila, P. Angsantikul, J. X. Li, M. A. Lopez-Ramirez, D. E. Ramírez-Herrera, S. Thamphiwatana, C. R. Chen, J. Delezuk, R. Samakapiruk, V. Ramez, L. F. Zhang, J. Wang, *Nat. Commun.* **2017**, *8*, 272.
[20] a) S. B. Liu, T. H. Zeng, M. Hofmann, E. Burcombe, J. Wei, R. R. Jiang, J. Kong, Y. Chen, *ACS Nano* **2011**, *5*, 6971 – 6980; b) L. Shi, J. R. Chen, L. J. Teng, L. Wang, G. L. Zhu, S. Liu, Z. T. Luo, X. T. Shi, Y. J. Wang, L. Ren, *Small* **2016**, *12*, 4265 – 4284; c) W. B. Hu, C. Peng, W. J. Luo, M. Lv, X. M. Li, D. Li, Q. Huang, C. H. Fan, *ACS Nano* **2010**, *4*, 4317 – 4323; d) J. J. Qiu, D. H. Wang, H. Geng, J. S. Guo, S. Qian, X. Y. Liu, *Adv. Mater. Interfaces* **2017**, *4*, 1700228; e) K. Krishnamoorthy, M. Veerapandian, L.-H. Zhang, K. Yun, S. J. Kim, *J. Phys. Chem. C* **2012**, *116*, 17280 – 17287.
[21] a) V. T. H. Pham, V. K. Truong, M. D. J. Quinn, S. M. Notley, Y. C. Guo, V. A. Baulin, M. Al Kobaisi, R. J. Crawford, E. P. Ivanova, *ACS Nano* **2015**, *9*, 8458 – 8467; b) X. F. Zou, L. Zhang, Z. J. Wang, Y. Luo, *J. Am. Chem. Soc.* **2016**, *138*, 2064 – 2077.
[22] a) Y. F. Mei, G. S. Huang, A. A. Solovev, E. B. Ureña, I. Monch, F. Ding, T. Reindl, R. K. Y. Fu, P. K. Chu, O. G. Schmidt, *Adv. Mater.* **2008**, *20*, 4085 – 4090; b) Y. F. Mei, A. A. Solovev, S. Sanchez, O. G. Schmidt, *Chem. Soc. Rev.* **2010**, *40*, 2109 – 2119.
[23] G. Wang, M. Zhang, Y. Zhu, G. Q. Ding, D. Jiang, Q. L. Guo, S. Liu, X. M. Xie, P. K. Chu, Z. F. Di, X. Wang, *Sci. Rep.* **2013**, *3*, 2465.
[24] R. Leancu, N. Moldovan, L. Csepregi, W. Lang, *Sens. Actuators A* **1995**, *46*, 35 – 37.
[25] V. M. Fomin, M. Hippler, V. Magdanz, L. Soler, S. Sanchez, O. G. Schmidt, *IEEE Trans. Rob.* **2014**, *30*, 40 – 48.
[26] a) I. D. Barcelos, L. A. B. Marçal, C. Deneke, L. G. Moura, R. G. Lacerda, A. Malachias, *RSC Adv.* **2016**, *6*, 103707 – 103713; b) G. M. Mao, Q. Wang, Z. E. Chai, H. Liu, K. Liu, X. M. Ren, *RSC Adv.* **2017**, *7*, 14481 – 14486; c) N. Ferralis, R. Maboudian, C. Carraro, *Phys. Rev. Lett.* **2006**, *97*, 187401.
[27] G. S. Huang, J. Wang, Y. F. Mei, *J. Mater. Chem.* **2012**, *22*, 6519 – 6525.
[28] S. Sanchez, A. N. Ananth, V. M. Fomin, M. Viehrig, O. G. Schmidt, *J. Am. Chem. Soc.* **2011**, *133*, 14860 – 14863.
[29] C. Jiang, G. S. Huang, S.-J. Ding, H. L. Dong, C. L. Men, Y. F. Mei, *Nanoscale Res. Lett.* **2016**, *11*, 289.
[30] J. X. Li, V. V. Singh, S. Sattayasamitsathit, J. Orozco, K. Kaufmann, R. F. Dong, W. Gao, B. Jurado-Sanchez, Y. Fedorak, J. Wang, *ACS Nano* **2014**, *8*, 11118 – 11125.

Manuscript received: February 28, 2019
Revised manuscript received: April 1, 2019
Accepted manuscript online: April 2, 2019
Version of record online: April 16, 2019